Dalton Transactions

Cite this: *Dalton Trans.*, 2012, **41**, 11642

www.rsc.org/dalton

PAPER

A new understanding on how heme metabolism occurs in heme oxygenase: water-assisted oxo mechanism†

Takashi Kamachi, Tomonori Nishimi and Kazunari Yoshizawa*

Received 10th April 2012, Accepted 18th June 2012
DOI: 10.1039/c2dt30777d

Heme metabolism by heme oxygenase (HO) is investigated with quantum mechanical/molecular mechanical (QM/MM) calculations. A mechanism assisted by water is proposed: (1) an iron–oxo species and a water molecule are generated by the heterolytic cleavage of the O–O bond of an iron–hydroperoxo species in a similar way to P450-mediated reactions, (2) a hydrogen atom abstraction by the iron–oxo species from the generated water molecule and the C–O bond formation between the water molecule and the α-*meso* carbon take place simultaneously. The water molecule is hydrogen-bonded to the oxo ligand and to the water cluster in the active site of HO. The water cluster can control the position of the generated water molecule to ensure the regioselective oxidation of heme at the α-*meso* position, at the same time, can facilitate the oxidation by stabilizing a positive charge on the water molecule in the transition state. A key difference between HO and P450 is observed in the structure of the active site; Thr252 in P450 blocks the access of the water molecule to the α-*meso* position, and can thus suppress the undesired heme oxidation for P450.

1. Introduction

Heme oxygenase (HO) catalyzes the conversion of heme to biliverdin, free iron ion and CO using O_2 and NADPH, as shown in Scheme 1.[1–3] In this process, the heme participates as both prosthetic group and substrate. In mammals, biliverdin is reduced by biliverdin reductase to bilirubin, which acts as a potent antioxidant. The iron released from the heme is essential for iron homeostasis because much of mammals' iron requirement is met by recycling this iron. CO has been suggested to serve as a signaling molecule in a manner analogous to NO.[4] All the products of the HO catalysis have important biological functions.

The first step of this catalytic reaction, the conversion of heme to α-*meso*-hydroxyheme, has been extensively investigated by both experimental and theoretical means. A generally accepted mechanism of the HO reaction consists of several steps; (1) binding to heme, (2) reduction of heme to lead to a ferrous species, (3) binding of molecular oxygen to the ferrous iron center and (4) the second electron transfer to form an active species that is responsible for the α-*meso* hydroxylation of heme. An iron–hydroperoxo species has been proposed to carry out the regioselective oxidation of heme at the α-*meso* position in the HO reaction. It was reported that HO reaction with ethyl hydroperoxide regioselectively yields α-*meso*-ethoxyheme.[5] This suggests that hydroxylation by the iron–hydroperoxo species proceeds in a concerted manner; the O–O bond cleavage and the O–C(α-*meso*) bond formation occur simultaneously, as shown in Fig. 1A. EPR and ENDOR measurements showed that one-electron reduction of an oxy form of the ferrous heme–HO complex by γ-ray at 77 K forms a ferric low-spin species that shows EPR characteristics of an iron–hydroperoxo species and then its decay leads to the formation of α-*meso*-hydroxyheme.[6] However, density functional theory (DFT) calculations showed that the concerted OH group transfer requires a very high activation energy of 170 kJ mol^{-1}, and therefore, two alternative mechanisms were proposed.[7,8] We proposed a water-assisted oxo mechanism, in which an iron–oxo species (iron(VI)–oxo porphyrin π-cation radical intermediate, the so-called compound I) and a water molecule are generated by the heterolytic cleavage of the O–O bond of the iron–hydroperoxo species in a similar way to P450-mediated reactions.[7] The water molecule produced is hydrogen-bonded to the oxo ligand and is placed in contact with the α-*meso* carbon atom. In the transition state, the hydrogen atom abstraction by the iron–oxo species from the bridging water molecule and the C–O bond formation occur simultaneously. The bridging water molecule greatly reduces the distortion of the porphyrin ring in the transition state, resulting in a remarkable decrease of the activation barrier to 58.2 kJ mol^{-1}. On the other hand, Shaik and co-workers[8] proposed a stepwise porphyrin degradation mechanism. This mechanism is initiated by the homolytic cleavage of the O–O bond of the hydroperoxo ligand, followed by the attack of the OH radical on α-*meso* carbon. Recently, they performed detailed QM/MM calculations[9] for the stepwise mechanism to characterize the role of the water

Institute for Materials Chemistry and Engineering and International Research Center for Molecular Systems, Kyushu University, Fukuoka 819-0395, Japan. E-mail: kazunari@ms.ifoc.kyushu-u.ac.jp; Fax: (+81)92-802-2528; Tel: (+81)92-802-2528

†Electronic supplementary information (ESI) available: Additional tables for computational results in this work. See DOI: 10.1039/c2dt30777d

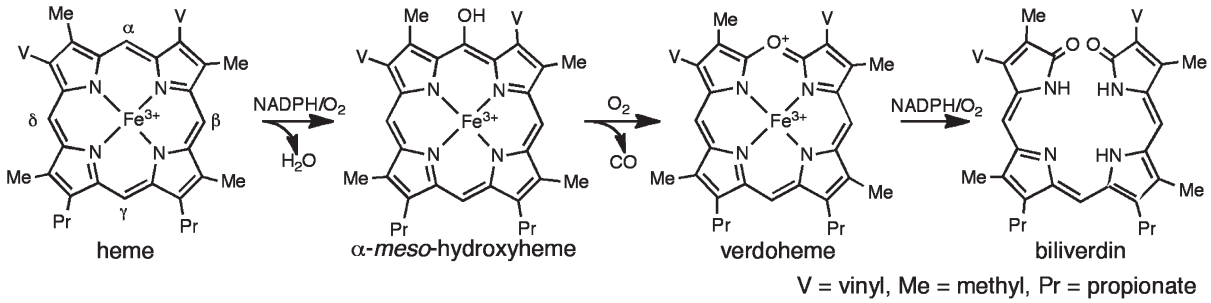

Scheme 1

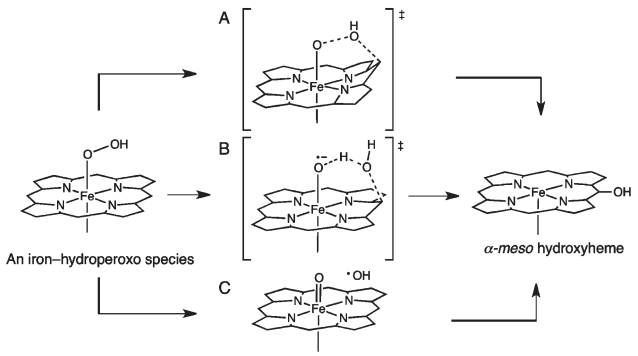

Fig. 1 Proposed mechanisms for heme oxidation by HO. (A) Concerted mechanism, (B) water-assisted oxo mechanism and (C) stepwise mechanism.

cluster in the distal pocket and showed that the activation energy of the O–O bond dissociation is 84 kJ mol^{-1} and the subsequent OH radical attack is barrierless.

The stepwise mechanism inevitably involves the formation of OH radical. It is well-known that OH radical generated in biological systems damages DNA and cell membranes.[10,11] Shaik and co-workers[9] concluded from the QM/MM calculations that a water cluster in the vicinity of the hydroperoxo ligand controls the movement of the OH radical to avoid its deleterious effects. We propose that heme oxidation can take place without involvement of OH radical in the water-assisted oxo mechanism.[7] However, Matsui *et al.*[12] examined reactions of HO with *m*-chloroperbenzoic acid (*m*CPBA) using a rapid-scan stopped-flow technique to show that an iron–oxo species generated by *m*CPBA in the active site of HO is reduced to compound II (iron(IV)–oxo neutral porphyrin intermediate) without heme oxidation. Our computational results[7b] indicate that the bridging water molecule plays a critical role in the oxidation reaction. The binding of *m*CPBA would disturb the hydrogen-bonding network involving the water cluster. Thus, the water-assisted oxo mechanism cannot be conclusively ruled out. In this study, we carried out QM/MM calculations to obtain better information on the structure and catalytic behavior of the iron–oxo species in the active site of HO.

2. Method of calculation

2-1. QM/MM model

To prepare a structurally reasonable model for QM/MM calculations, we did initial model setting on the basis of the crystal structure[13] (PDB ID 1IVJ) of rat hemeoxygenase-1 complexed with heme and azide. Protonation states of titratable residues at pH 7.0 were determined by using the pK_a prediction method, which is based on the theory developed by Bashford and Karplus.[14] This method combines electrostatic energy calculations based on the Generalized Born approximation[15] with an iterative mobile clustering approach to calculate the equilibria of proton binding to multiple titration sites in protein molecules.[16] The use of the iterative mobile clustering is an effective way to treat the combinatorial problem arising from the exponential growth of protonation states with the number of titratable groups. The enzyme model thus obtained was solvated by a sphere of water molecules with a radius of 30 Å, in which 2247 TIP3P[17] water molecules were added. The final system contains the model protein, substrate and 2433 water molecules, leading to 10819 atoms in total. The system was heated and equilibrated with the CHARMm force field developed by Momany and Rone[18] in three steps: (i) steepest descent optimization of the system, (ii) molecular dynamics (MD) for 15 ps heating from 50 to 300 K and (iii) equilibration for 400 ps at 300 K with a timestep of 1 fs. The non-bonded cutoff radius was set to be 14 Å in the MD simulations. During the CHARMM[19] MD simulation the coordinates of the QM-region atoms were kept fixed. The SHAKE algorithm[20] was used to constrain bonds involving hydrogen atoms. Finally, the system was minimized with the adopted basis Newton–Raphson (ABNR) algorithm[21] for 5000 steps without any cutoff for non-bonded interactions. All calculations were carried out with Discovery Studio 2.0.[22]

2-2. QM/MM calculations

The bridging water molecule is hydrogen-bonded to the oxo ligand of the iron–oxo species and the water cluster composed of the four water molecules (W1–W4), as discussed in detail in section 3-1. The QM region includes the iron–oxo porphyrin complex (without side chains of heme), the imidazole moiety of His25 and the five water molecules. Link atoms were introduced to saturate the valence of the QM boundary atoms with the L2 scheme,[23] where the link atoms do not interact with the MM atoms of the adjacent neutral charge group. All QM/MM calculations were performed with the ChemShell package[24] by using TURBOMOLE[25] for the QM calculations at the B3LYP level of theory, which consists of the Slater exchange, the Hartree–Fock exchange, the exchange functional of Becke,[26] the correlation functional of Lee, Yang, and Parr (LYP)[27] and the correlation

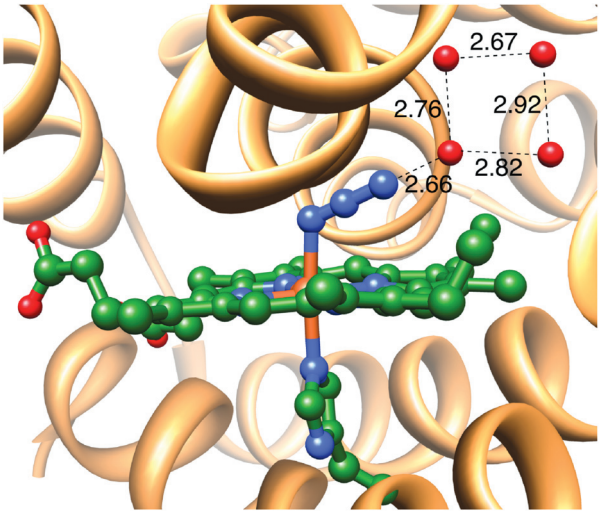

Fig. 2 The active site of heme oxygenase complexed with heme and azide (PDB ID 1IVJ). The azide ligand is hydrogen-bonded to a water cluster in the crystal structure.[13] Units in Å.

functional of Vosko, Wilk and Nusair.[28] The basis set of choice is SV(P)[29] for all atoms to carry out geometry optimizations. The CHARMm force field[18] run through the DL_POLY program[30] was used for the MM part of the system. A standard electronic embedding scheme[31] was chosen: the fixed MM atomic charges were included into the one-electron Hamiltonian of the QM calculations, and the QM/MM electrostatic interactions were evaluated from the QM electrostatic potential and the MM atomic charges. No cutoffs were applied for the nonbonded MM and QM/MM interactions. We defined a region with 783 atoms to be fully optimized by including all residues that have atoms within a distance of 10 Å around any atom of substrate, while we kept the remaining atoms fixed. Vibrational frequencies were numerically computed for all stationary points in order to confirm that each optimized geometry corresponds to a local minimum that has no imaginary frequency or to a saddle point that has only one imaginary frequency.

3. Results and discussion

Noguchi and coworkers[13] determined the crystal structure of rat HO-1 complexed with heme and azide at 1.9 Å resolution, as shown in Fig. 2. The distance between the azide and the iron atom of heme is 2.2 Å. The azide ligand is nearly parallel to the heme plane and directed toward the α-*meso* carbon. Raman spectroscopic analyses suggested that the binding mode of azide provides a reasonable model of dioxygen and hydroperoxide binding to the heme in HO. The azide ligand interacts with Arg136 and Asp140 *via* several water molecules in the crystal structure. The hydrogen-bonding network fixes the azide ligand in a proper position for the OH group attack to the α-*meso* carbon. They proposed that the water molecules can also play important roles in the protonation and activation of peroxide bound to heme. To examine the role of the water cluster in the water-assisted oxo mechanism, we consider effects of the water cluster on the activation energy using a simplified model involving the iron–oxo porphine complex and one or two water molecules in section 3-1. We discuss the water-assisted heme oxidation by the iron–oxo species in the protein environment using the QM/MM calculations in section 3-2.

3-1. Catalytic effects of the water cluster

Fig. 3A shows computed energies and optimized geometries for heme oxidation by the iron–oxo species with the aid of one water molecule in the doublet and quartet state at the B3LYP/TZVP[32]//B3LYP/SV(P) level of theory. Calculated atomic charges and spin densities are listed in Table 1. In the starting geometry for optimization, we placed a water molecule at the same position as the terminal N atom of the azide ligand assuming that the water molecule is generated by the heterolytic cleavage of the O–O bond of the iron–hydroperoxo species. The water molecule forms hydrogen-bond bridges between the oxo ligand and the α-*meso* carbon in the optimized structure of the reactant complex; the oxo ligand holds the water molecule through a hydrogen bond of 1.886 Å. The distance between the oxygen atom of the water molecule and the *meso*-carbon atom is 2.862 (2.861) Å in the doublet (quartet) state. An O–H bond cleavage and a C–O bond formation occur simultaneously in this mechanism. This transition state has only one imaginary frequency mode of 447i (449i) cm^{-1} in the doublet (quartet) state, which corresponds to O–H and C–O stretching motions. The O–H bond of the water molecule and the C–O bond are 1.081 (1.082) Å and 1.822 (1.821) Å in the doublet (quartet) state, respectively. A calculated activation energy for this step is 65.3 (64.9) kJ mol^{-1} in the doublet (quartet) state, and it is 113.0 kJ mol^{-1} lower than the corresponding value for the direct oxo attack in the absence of the bridging water molecule.[7] These results support our idea that a bridging water molecule facilitates the OH group transfer to the *meso* carbon through a less-strained transition state in the oxo mechanism. The transition state leads to the formation of an intermediate with a hydrogen bond between the OH ligand and the migrated OH group. The overall reaction is 61.1 and 20.5 kJ mol^{-1} exothermic on the doublet and quartet surfaces, respectively, which indicates that the reaction should mainly proceed on the doublet potential energy surface. This is reasonable because low-spin states are preferred for the six-coordinate Fe(III) complexes. To assess the reliability of the method in describing the oxidation process, we carried out single-point calculations with the 6-311G(d,p)[33] and cc-pVTZ[34] basis sets and the M06[35] and CAM-B3LYP[36] functionals. The calculated activation barriers are not sensitive to the choice of basis sets and density functionals although the reaction is predicted to be more exothermic in the M06 and CAM-B3LYP calculations (Table S1†).

As shown in Fig. 2, the terminal N atom of the azide ligand is hydrogen-bonded to a water molecule of the water cluster. Thus, the bridging water molecule would form a hydrogen bond with the water cluster in the active site of the enzyme. To evaluate effects of the hydrogen bonding interaction, we calculated the activation energy for the water-assisted oxo mechanism in the presence of an additional water molecule, as shown in Fig. 3B. The water molecule is hydrogen-bonded to the bridging water molecule. The distance between the oxygen atom of the bridging

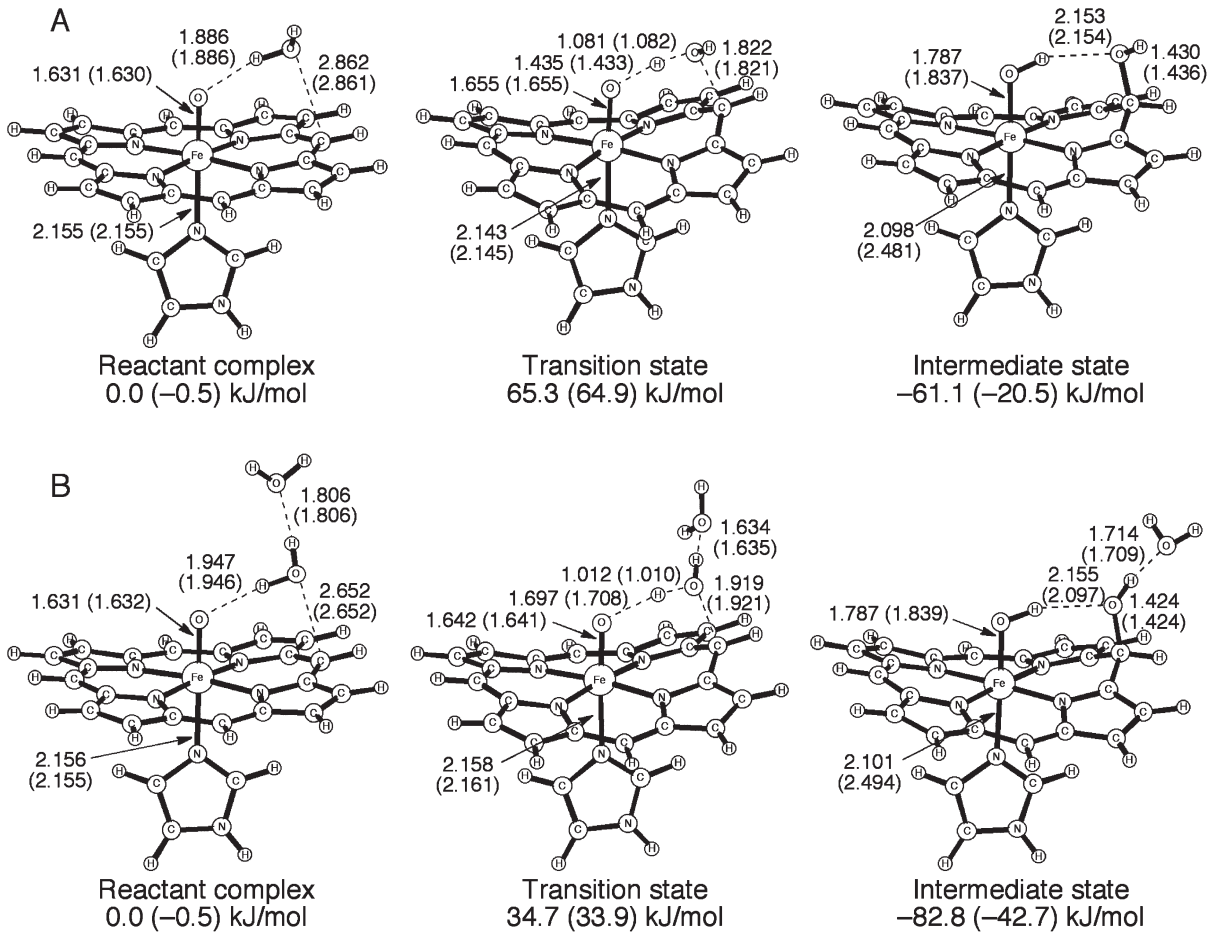

Fig. 3 Computed geometric and energetic changes in heme oxidation by the iron–oxo species with the aid of one or two water molecules in the doublet (quartet) state. Unit in Å. (A) One water model and (B) two water model.

Table 1 Calculated Mulliken charges (spin densities) on the small model calculations. RC, TS and I stands for reactant complex, transition state and intermediate, respectively

	Fe	O (oxo)	Bridging HOH	Imidazole	Porphyrin	Additional HOH
Doublet state with the bridging water molecule						
RC	0.2 (1.2)	−0.3 (0.9)	0.0 (0.0)	0.3 (0.0)	0.7 (−1.1)	—
TS	0.2 (1.4)	−0.3 (0.7)	0.3 (−0.1)	0.4 (0.0)	0.5 (−1.0)	—
I	0.3 (0.9)	−0.4 (0.2)	0.3 (0.0)	0.3 (0.0)	0.6 (−0.1)	—
Quartet state with the bridging water molecule						
RC	0.2 (1.2)	−0.3 (0.9)	0.0 (0.0)	0.3 (0.0)	0.7 (0.9)	—
TS	0.2 (1.4)	−0.3 (0.6)	0.3 (0.1)	0.4 (0.0)	0.5 (0.9)	—
I	0.5 (2.6)	−0.5 (0.4)	0.3 (0.0)	0.2 (0.0)	0.6 (0.0)	—
Doublet with the bridging and additional water molecule						
RC	0.2 (1.2)	−0.3 (0.9)	0.0 (0.0)	0.3 (0.0)	0.7 (−1.0)	0.0 (0.0)
TS	0.2 (1.3)	−0.3 (0.8)	0.3 (−0.1)	0.3 (0.0)	0.4 (−1.0)	0.1 (0.0)
I	0.2 (0.9)	−0.4 (0.2)	0.2 (0.0)	0.3 (0.0)	0.5 (−0.1)	0.1 (0.0)
Doublet with the bridging and additional water molecule						
RC	0.2 (1.2)	−0.3 (0.9)	0.0 (0.0)	0.3 (0.1)	0.7 (0.9)	0.0 (0.0)
TS	0.2 (1.3)	−0.3 (0.8)	0.3 (0.1)	0.3 (0.0)	0.4 (0.8)	0.1 (0.0)
I	0.5 (2.6)	−0.5 (0.4)	0.2 (0.0)	0.2 (0.0)	0.6 (0.0)	0.1 (0.0)

water molecule and the *meso*-carbon atom decreases by 0.21 Å in the presence of the water molecule that mimics the water cluster at the active site of HO. This result indicates that the bridging water molecule tightly interacts with the *meso*-carbon atom and that the water attack is structurally favored in the active site of HO. The transition state for the attack has a lower imaginary frequency of 254i (249i) cm^{-1} in the doublet (quartet) state, which indicates that the hydrogen-bonding interaction can

weaken the O–H bond of the bridging water. The calculated activation barrier of the attack is 34.7 (33.9) kJ mol^{-1}, and the overall reaction is 82.8 (42.7) kJ mol^{-1} exothermic in the doublet (quartet) spin state. The significant decrease in the activation barrier is likely to be due to the hydrogen-bonding interaction between the bridging and additional water molecules in the transition state. As shown in Fig. S1,† the effect of the third water molecule is negligible. The hydrogen bond between the bridging and additional water molecules is shortened by 0.17 Å in comparison with that in the reactant complex. As listed in Table 1, the charge of the bridging water changes from 0.0 in the reactant complex to 0.3 in the transition state. The positive charge localized on the bridging water molecule is stabilized by the strong hydrogen bond with the additional water molecule so that the heme oxidation proceeds easier. From these results, we conclude that the iron–oxo species can act as the active species responsible for the heme oxidation with the aid of the bridging water molecule and that the water cluster in the active site facilitates the reaction further.

3-2. QM/MM analysis of the water-assisted oxo mechanism inside the enzyme

We set up a whole-enzyme model for the iron–oxo species from the crystal structure[13] by replacing the azide ligand with the oxo ligand and the bridging water molecule. Fig. 4 shows a QM/MM optimized structure of the reaction intermediates and the transition state in heme oxidation mediated by the iron–oxo species of HO. Calculated Mulliken charges and spin densities are listed in Table 2. Five water molecules (W1–W5) are involved in the QM region because the water molecules are crucial for the proper catalytic function of HO. These important water molecules were included in the QM region in the previous QM/MM studies[7b,9] on this enzyme. The water molecule (W5) eliminated from the iron–hydroperoxo species is hydrogen-bonded to the oxo ligand and to W1 in the water cluster. The hydrogen bond between the oxo ligand and the bridging water molecule is 2.060 (2.054) Å in length and the hydrogen bond distance between the bridging water molecule and W1 is 1.822 (1.830) Å in the doublet (quartet) state. These distances for the QM/MM optimized structure are close to those of the reactant complex that involves only the iron–oxo complex and the two water molecules. The spin densities of the iron atom, the oxo ligand, and the porphyrin ring were calculated to be 1.3 (1.2), 0.8 (0.8) and −1.1 (0.9), respectively, in the doublet (quartet) state. This result shows that the Fe–O moiety of the iron–oxo species has two unpaired parallel-spin electrons, which are weakly coupled with one unit of spin located on the porphyrin ring. Thus, the doublet and quartet potential energy surfaces are close lying in the initial stages of the reaction.

The optimized structure of the transition state has the O_{W5}–H bond of 1.050 (1.048) and the C–O_{W5} bond of 1.772 (1.772) Å in the doublet (quartet) state. This transition state in the doublet (quartet) state has only one imaginary frequency mode of 270i (259i) cm^{-1}, which corresponds to C–O and O–H stretching motions. A calculated activation energy for this step is 76 kJ mol^{-1} in the doublet and quartet states, this value being about 42 kJ mol^{-1} higher than that for the small model calculation with the two water molecules. We divided the QM/MM energies into the QM and MM parts to find the main reason of the energy difference, as listed in Table 3. The QM energy can be further divided into two contributions, one coming from the geometrical change of the QM region in the course of reaction and the other one from the polarization of the QM region in response to the MM point charges. These components are estimated by performing single-point calculations of the QM system in the gas phase without point charges. We see that the electrostatic interactions between the QM and MM regions can significantly increase the activation energy by about 39 kJ mol^{-1}. As listed in Table S2,† we considered coulomb interactions between the QM charges and the MM point charges to determine which part of the system has large electrostatic effects on the destabilization of the transition state. This computational result shows that the increase of the barrier in the QM/MM calculations is mainly ascribed to MM point charges on the side chains of heme, especially, propionate groups. To estimate the impact of the side chains on the QM/MM energy, we performed single-point calculations with a larger QM region including the side chains, as summarized in Table S3.† The QM/MM energy differences between the larger and smaller QM models are calculated to be less than 8.8 kJ mol^{-1}. This result suggests that the smaller model is appropriate in describing the oxidation process and that the barrier height for this reaction is increased in the presence of the side chains of heme.

The transition state leads to the formation of an intermediate with an intramolecular hydrogen bond between the OH ligand and the migrated OH group. The spin density of the iron atom of the intermediate is calculated to be 1.0 (2.7) in the doublet (quartet) state, which indicates that the formal charge of the iron atom is +3. Since six-coordinate ferric complexes are most stable in the low-spin state, the doublet state is 38.3 kJ mol lower than the quartet state. The overall reaction is 77.7 and 39.4 kJ mol^{-1} exothermic in the doublet and quartet states, respectively. Thus, this reaction can proceed on the doublet potential energy surface. The water cluster retains its shape and appears to be stable in the course of the reaction. Thus, the water cluster serves as an anchor for the bridging water molecule, and consequently, the bridging water molecule exclusively attacks the α-*meso* position in heme activation. In this mechanism, we assumed that the distal oxygen of the iron–hydroperoxo species is retained in the OH group of α-*meso*-hydroxyheme. Thus, the oxidation of the porphyrin ring would take place without the exchange of the bridging water molecule with solvent.

4. Discussion

We have shown from the QM/MM computations that the water-assisted oxo mechanism is operative even in the protein environment of HO. The calculated activation energy is comparable to that for the stepwise mechanism[8] and is much lower than that for the concerted mechanism.[5] However, the iron–oxo species formed in P450s has never been reported to oxidize its α-*meso* carbons although water molecules are accessible to the active site. Closer inspection of crystal structures available for P450s reveals a significant, common structural motif relating all of these enzymes. In the vicinity of the β-, γ- and δ-*meso* carbons

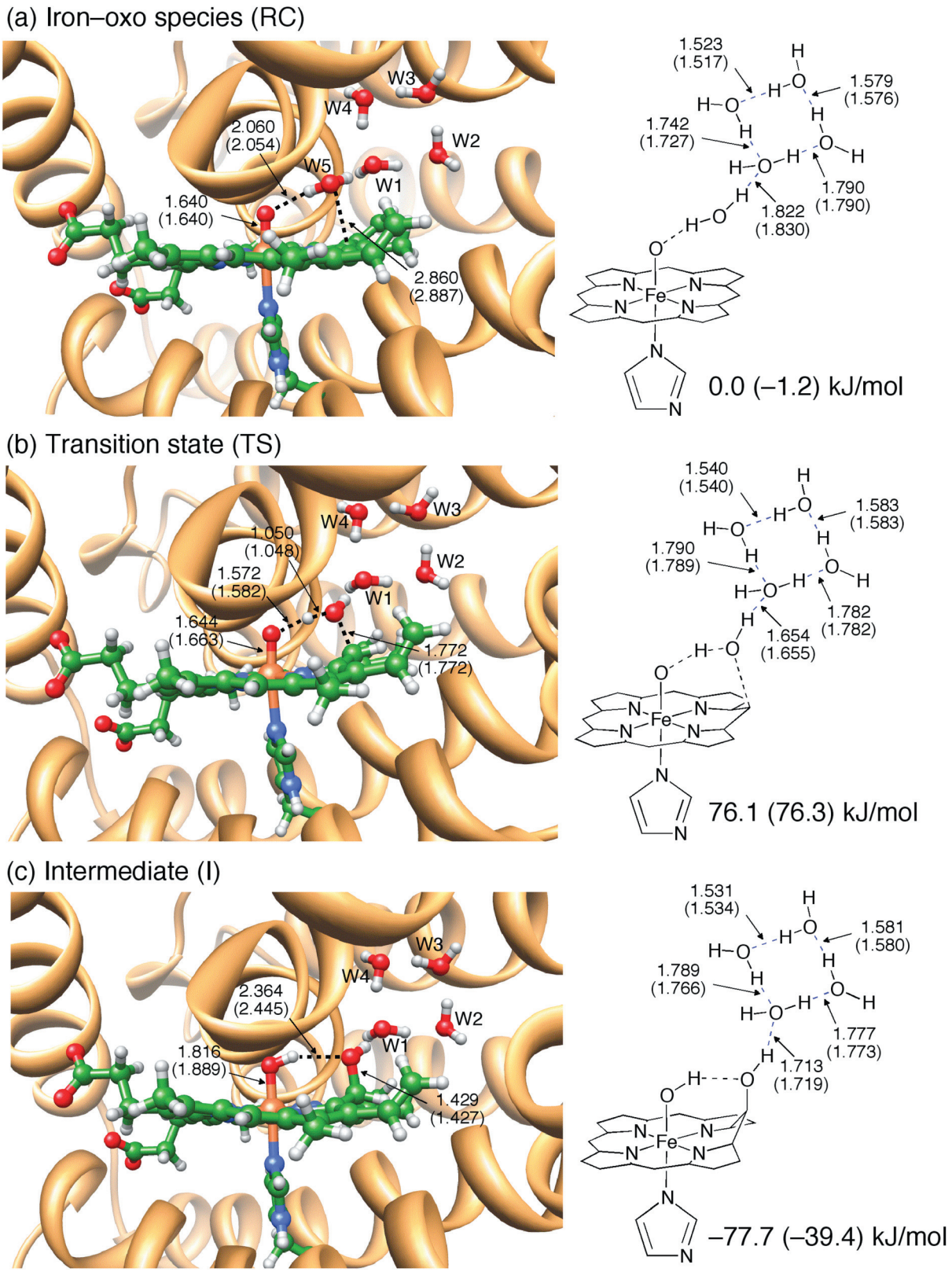

Fig. 4 Computed energetic and structural changes in heme oxidation by the iron–oxo species of HO with the aid of a water molecule in the protein environment in the doublet (quartet) states. Bond distances in Å.

of heme, hydrophobic amino acids or substrates are present in the distal heme pocket at an average distance of ~4 Å, as summarized in Table S4.† Water molecules tend to avoid the hydrophobic amino acids and the bound substrate lies above the *meso* carbons, which prevents the bridging water molecule from attacking the β-, γ-, and δ-*meso* carbons of heme.

Table 2 Calculated Mulliken charges (spin densities) of the Fe and O atoms, the imidazole and the porphyrin moieties, and five water molecules which construct the hydrogen bonding network for heme oxidation mediated by the iron–oxo species of HO

	Fe	O (oxo)	W5	Imidazole	Porphyrin	W1– W4
Doublet						
RC	0.2 (1.3)	−0.3 (0.8)	0.0 (0.0)	0.3 (0.0)	0.8 (−1.1)	0.0 (0.0)
TS	0.2 (1.5)	−0.4 (0.6)	0.3 (−0.1)	0.3 (0.0)	0.5 (−1.1)	0.1 (0.0)
I	0.3 (1.0)	−0.5 (0.1)	0.3 (0.0)	0.3 (0.0)	0.6 (−0.1)	0.1 (0.0)
Quartet						
RC	0.2 (1.2)	−0.3 (0.8)	0.0 (0.0)	0.3 (0.0)	0.8 (0.9)	0.0 (0.0)
TS	0.2 (1.4)	−0.4 (0.6)	0.3 (0.1)	0.3 (0.0)	0.5 (0.9)	0.1 (0.0)
I	0.5 (2.7)	−0.6 (0.3)	0.3 (0.0)	0.2 (0.0)	0.6 (−0.1)	0.1 (0.0)

Table 3 QM/MM and QM energies (kJ mol^{-1}) measured from RC

	QM/MM	QM	MM	QM (gas)
RC	0.0 (−1.2)	0.0 (−1.0)	0.0 (−0.2)	0.0 (0.0)
TS	76.1 (76.3)	88.5 (88.8)	−12.4 (−12.6)	49.4 (49.4)
I	−77.7 (−39.4)	−70.4 (−36.3)	−7.3 (−3.1)	−72.0 (−30.1)

On the other hand, the closest amino acid to the α-*meso* carbons is threonine, which is considered to be a key residue for the proton donation in P450s. Mutational studies of P450cam indicated that the Thr252Ala mutation results in a significant decrease of hydroxylation ability.[37] A proton inventory analysis of experimental kinetic solvent isotope effect (KSIE) data showed that at least two protons are involved in the formation of the iron–oxo species of P450 and proposed a possible proton delivery model for P450cam involving Asp251, Thr252 and two water molecules.[38] In a previous study, we performed DFT calculations to elucidate the mechanism of the formation of the iron–oxo species of P450cam using this proton source model.[39] The proton transfer process is highly exothermic, and thus these hydrogen bond networks can promote effective proton donation to the distal oxygen. In the active site of HO, the essential water cluster is hydrogen-bonded to Arg136 and Asp140 that can render or pass a proton for the heterolytic cleavage of the O–O bond. The iron–oxo species is responsible for C–H bond activation in P450s. Recently, Rittle and Green[40] successfully prepared the iron–oxo species in 75% yield by reacting CYP119 with *m*-chloroperbenzoic acid and measured the reaction rate at which the iron–oxo species hydroxylates inert hydrocarbons. A large observed KIE of 12.5 is consistent with the so-called oxygen rebound mechanism,[41] in which the iron–oxo species abstracts hydrogen from the substrate, which is followed by the recombination of the resultant radical species to form the hydroxylated product. HO includes a similar hydrogen-bonding network in the active site; the distal oxygen of the peroxo ligand is bridged to Arg136 and Asp140 by two water molecules in the water cluster. The carboxylate anion of Asp140 is hydrogen-bonded to the side chain of Arg136, and the two water molecules are arranged between the COO^- moiety of Asp140 and the distal oxygen. The carboxylate at position 140 is essential to activate the iron-bound dioxygen and hydroperoxide.[42] The features of the hydrogen-bonding network in the active site are likely to be shared between P450s and HO, and therefore, such a proton transfer mechanism can work in the active site of HO to give the iron–oxo species, which can act as an active species of heme oxidation.

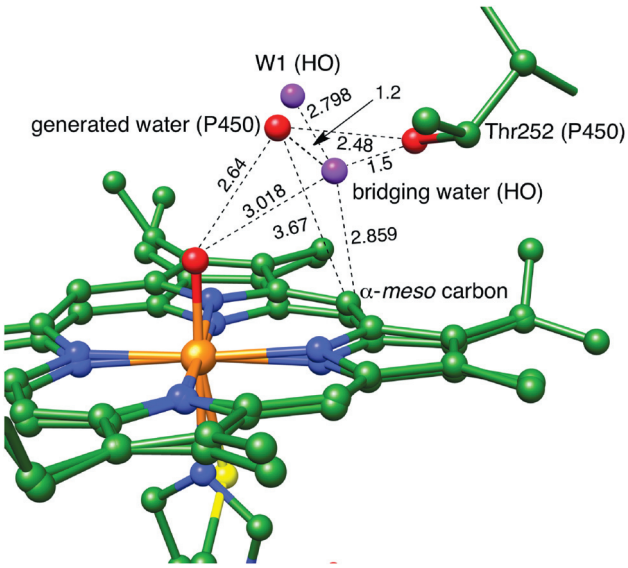

Fig. 5 Close up of the superimposition of the iron–oxo species in the QM/MM-optimized structure of HO and in the crystal structure (1DZ9) of P450. Key water molecules (purple in HO and red in P450) and Thr252 in P450 are also displayed. Distances in Å.

Schlichting *et al.*[43] reported that the irradiation of the ferrous dioxygen adduct of P450cam with 1.5 Å X-rays results in breakdown of the dioxygen molecule to an intermediate that is consistent with the iron–oxo species. In the crystal structure (PDB ID 1DZ9), a single oxygen atom is bound to the Fe atom of heme at 1.65 Å distance. There is a water molecule close to the oxo ligand (2.64 Å) and the hydroxyl group of Thr252 (2.48 Å), which might be generated by the cleavage of the O–O bond. This crystal structure provided an important clue to the question why P450s do not catalyze heme oxidation. We superimposed the porphyrin rings and the generated water molecule extracted from the crystal structure and from the QM/MM-optimized structure of the iron–oxo species of HO in Fig. 5. This figure clearly shows that the distance between the generated water molecule and the α-*meso* carbon is shorter in HO than that in P450cam; 2.859 Å in HO and 3.67 Å in P450. The generated water molecule in P450 has to move by ~1.2 Å toward the position of bridging water in HO to attack the α-*meso* carbon. However, this position is not accessible to the water molecule in P450, due to

the steric effect of Thr252; the distance between the hydroxyl group of Thr252 and the position of bridging water in HO is only 1.5 Å. Very recently, Shaik and co-workers[44] investigated from QM/MM calculations to determine why the Phe429His mutant of cytochrome P450 2B4 acquires an ability to oxidize heme. In the optimized structure of the mutant, the hydrogen-bonding network for proton delivery is significantly perturbed by the mutation. In particular, Thr302 is oriented away from the α-*meso* carbon, the distance between Oγ of Thr302 and the α-*meso* carbon being 3.589 and 4.864 Å in the wild-type enzyme and the mutant, respectively. This would increase the vulnerability to the heme degradation in the mutant. The active site of P450s is designed to prevent potential side reactions by repelling water molecules away from the *meso* positions of heme.

5. Conclusions

We performed QM and QM/MM calculations to re-examine the water-assisted oxo mechanism of heme oxidation mediated by heme oxygenase proposed in a previous study.[7] In this mechanism, the hydrogen atom abstraction by the iron–oxo species from a bridging water molecule and the C–O bond formation between the bridging water molecule and the α-*meso* carbon take place simultaneously. The bridging water molecule is hydrogen-bonded to the water cluster in the crystal structure of HO. We estimated the effect of the water cluster on the activation energy using a simplified model including the iron–oxo complex, the bridging and an additional water molecule. The additional water molecule significantly reduces the barrier because the additional water stabilizes the positive charge localized on the bridging water molecule in the transition state. We built a whole-enzyme model with 10819 atoms to gain a better understanding of effects of the water cluster. The QM region of our QM/MM model involves an iron–oxo complex and five water molecules to reproduce the important hydrogen-bonding network. In the QM/MM-optimized structure of the iron–oxo species, the bridging water molecule and the water cluster form a hydrogen-bonding network that connects the oxo ligand. The structural features of the hydrogen-bonding network are similar to the proton delivery system of P450 for the conversion of the iron–peroxo species to the iron–oxo species. The calculated activation energy is 76 kJ mol^{-1} for the heme oxidation with the bridging water molecule in the QM/MM calculations. Our QM/MM results suggest that the heterolytic cleavage of the O–O bond of the iron–hydroperoxo species and the heme oxidation with the aid of the bridging water molecule can take place under physiological conditions. The iron–oxo species acts as an active species in the P450-mediated reactions, but does not bring about the oxidation of the α-*meso* carbon. This is likely to be because the water molecule generated by the cleavage of the O–O bond is not accessible to the *meso* carbons of heme in P450 due to the surrounding amino acids in the active site.

Acknowledgements

We thank Grants-in-Aid for Scientific Research (No. 22245028) from the Japan Society for the Promotion of Science (JSPS) and the Ministry of Education, Culture, Sports, Science and Technology of Japan (MEXT), the Kyushu University Global COE Project "Molecular Systems Chemistry", the Nanotechnology Support Project, the MEXT Project of Integrated Research on Chemical Synthesis, and CREST of the Japan Science and Technology Cooperation.

References

1 (*a*) P. R. Ortiz de Montellano, *Acc. Chem. Res.*, 1998, **31**, 543; (*b*) P. R. Ortiz de Montellano, *Curr. Opin. Chem. Biol.*, 2000, **4**, 221; (*c*) C. Colas and P. R. Ortiz de Montellano, *Chem. Rev.*, 2003, **103**, 2305.
2 T. Yoshida and C. T. Migita, *J. Inorg. Biochem.*, 2000, **82**, 33.
3 (*a*) M. Unno, T. Matsui and M. Ikeda-Saito, *Nat. Prod. Rep.*, 2007, **24**, 553; (*b*) T. Matsui, M. Unno and M. Ikeda-Saito, *Acc. Chem. Res.*, 2010, **43**, 240.
4 T. R. Johnson, B. E. Mann, J. E. Clark, R. Foresti, C. J. Green and R. Motterlini, *Angew. Chem., Int. Ed.*, 2003, **42**, 3722.
5 (*a*) A. Wilks and P. R. Ortiz de Montellano, *J. Biol. Chem.*, 1993, **268**, 22357; (*b*) A. Wilks, J. Torpey and P. R. Ortiz de Montellano, *J. Biol. Chem.*, 1994, **269**, 29553.
6 (*a*) R. M. Davydov, T. Yoshida, M. Ikeda-Saito and B. M. Hoffman, *J. Am. Chem. Soc.*, 1999, **121**, 10656; (*b*) R. Davydov, V. Kofman, H. Fujii, T. Yoshida, M. Ikeda-Saito and B. M. Hoffman, *J. Am. Chem. Soc.*, 2002, **124**, 1798.
7 (*a*) T. Kamachi, A. F. Shestakov and K. Yoshizawa, *J. Am. Chem. Soc.*, 2004, **126**, 3672; (*b*) T. Kamachi and K. Yoshizawa, *J. Am. Chem. Soc.*, 2005, **127**, 10686.
8 (*a*) P. K. Sharma, R. Kevorkiants, S. P. de Visser, D. Kumar and S. Shaik, *Angew. Chem., Int. Ed.*, 2004, **43**, 1129; (*b*) D. Kumar, S. P. de Visser and S. Shaik, *J. Am. Chem. Soc.*, 2005, **127**, 8204.
9 H. Chen, Y. Moreau, E. Derat and S. Shaik, *J. Am. Chem. Soc.*, 2008, **130**, 1953.
10 B. Halliwell, *FASEB J.*, 1987, **1**, 358.
11 O. I. Aruoma, B. Halliwell, E. Gajewski and M. Dizdaroglu, *J. Biol. Chem.*, 1989, **264**, 20509.
12 T. Matsui, S. H. Kim, H. Jin, B. M. Hoffman and M. Ikeda-Saito, *J. Am. Chem. Soc.*, 2006, **128**, 1090.
13 M. Sugishima, H. Sakamoto, Y. Higashimoto, Y. Omata, S. Hayashi, M. Noguchi and K. Fukuyama, *J. Biol. Chem.*, 2002, **277**, 45086.
14 D. Bashford and M. Karplus, *J. Phys. Chem.*, 1991, **95**, 9556.
15 B. N. Dominy and C. L. Brooks III, *J. Phys. Chem. B*, 1999, **103**, 3765.
16 V. Z. Spassov and L. Yan, *Protein Sci.*, 2008, **17**, 1955.
17 W. L. Jorgensen, J. Chandrasekhar, J. D. Madura, R. W. Impey and M. L. Klein, *J. Chem. Phys.*, 1983, **79**, 926.
18 (*a*) F. A. Momany and R. Rone, *J. Comput. Chem.*, 1992, **13**, 888; (*b*) F. A. Momany, R. Rone, H. Kunz, R. F. Frey, S. Q. Newton and L. Schäfer, *J. Mol. Struct. (THEOCHEM)*, 1993, **286**, 1.
19 B. R. Brooks, R. E. Bruccoleri, B. D. Olafson, D. J. States, S. Swaminathan and M. Karplus, *J. Comput. Chem.*, 1983, **4**, 187.
20 J. Ryckaert, G. Ciccotti and H. J. C. Berendsen, *J. Comput. Phys.*, 1977, **23**, 327.
21 W. H. Press, B. P. Flannery, S. A. Teukolshy and W. T. Vetrrling, *Numerical Recipes: The Art of Scientific Computing*, University Press, Cambridge, 1987.
22 *Discovery Studio 2.0*, Accelrys Software Inc., San Diego, 2007.
23 I. Antes and W. Thiel, in *Hybrid Quantum Mechanical and Molecular Mechanical Methods*, ed. J. Gao, ACS Symposium Series 712, American Chemical Society, Washington, D.C., 1998, pp. 50–65.
24 *ChemShell, a Computational Chemistry Shell*, see www.chemshell.org.
25 R. Ahlrichs, M. Bär, M. Häser, H. Horn and C. Kölmel, *Chem. Phys. Lett.*, 1989, **162**, 165.
26 (*a*) A. D. Becke, *Phys. Rev. A: At., Mol., Opt. Phys.*, 1988, **38**, 3098; (*b*) A. D. Becke, *J. Chem. Phys.*, 1993, **98**, 5648.
27 C. Lee, W. Yang and R. G. Parr, *Phys. Rev. B*, 1988, **37**, 785.
28 S. H. Vosko, L. Wilk and M. Nusair, *Can. J. Phys.*, 1980, **58**, 1200.
29 A. Schäfer, H. Horn and R. Ahlrichs, *J. Chem. Phys.*, 1992, **97**, 2571.
30 W. Smith and T. R. Forester, *J. Mol. Graphics*, 1996, **14**, 136.
31 D. Bakowies and W. Thiel, *J. Phys. Chem.*, 1996, **100**, 10580.
32 A. Schäfer, C. Huber and R. Ahlrichs, *J. Chem. Phys.*, 1994, **100**, 5829.
33 R. Krishnan, J. S. Binkley, R. Seeger and J. A. Pople, *J. Chem. Phys.*, 1980, **72**, 650.

34 R. A. Kendall, T. H. Dunning and R. J. Harrison, *J. Chem. Phys.*, 1992, **96**, 6796.
35 Y. Zhao and D. G. Truhlar, *Theor. Chem. Acc.*, 2007, **120**, 215.
36 T. Yanai, D. P. Tew and N. C. Handy, *Chem. Phys. Lett.*, 2004, **393**, 51.
37 S. A. Martinis, W. M. Atkins, P. S. Stayton and S. G. Sligar, *J. Am. Chem. Soc.*, 1989, **111**, 9252.
38 M. Vidakovic, S. G. Sligar, H. Li and T. L. Poulos, *Biochemistry*, 1998, **37**, 9211.
39 T. Kamachi and K. Yoshizawa, *J. Am. Chem. Soc.*, 2003, **125**, 4652.
40 J. Rittle and M. T. Green, *Science*, 2010, **330**, 933.
41 (*a*) J. T. Groves, R. C. Haushalter, M. Nakamura, T. E. Nemo and B. J. Evans, *J. Am. Chem. Soc.*, 1981, **103**, 2884; (*b*) J. T. Groves, *J. Chem. Educ.*, 1985, **62**, 928.
42 H. Fujii, X. Zhang, T. Tomita, M. Ikeda-Saito and T. Yoshida, *J. Am. Chem. Soc.*, 2001, **123**, 6475.
43 I. Schlichting, J. Berendzen, K. Chu, A. M. Stock, S. A. Maves, D. E. Benson, R. M. Sweet, D. Ringe, G. A. Petsko and S. G. Sligar, *Science*, 2000, **287**, 1615.
44 D. Usharani, C. Zazza, W. Lai, M. Chourasia, L. Waskell and S. Shaik, *J. Am. Chem. Soc.*, 2012, **134**, 4053.